CONTENTS

Abstract ii
Problem Status ii
Authorization ii

INTRODUCTION 1

THEORY 1

EXPERIMENTAL MEASUREMENTS 3
Area of Operations 3
Instrumentation 4
Procedure and Geometry 4

ANALYSIS AND RESULTS 5
Treatment of Measured Data 5
Scattered Field 6
Ratio of Scattered to Incident Power 9

SUMMARY AND CONCLUSIONS 10

ACKNOWLEDGEMENT 10

REFERENCES 11

APPENDIX A — Effects of Propagation 12

APPENDIX B — Monitoring Positions by Acoustic Means 13

APPENDIX C — Three-Dimensional Data 16

ABSTRACT

An experiment to determine the three-dimensional acoustic field scattered from the sea bottom was conducted in the Blake Plateau. Pulsed 19.5-kHz transmissions were directed toward the bottom from a submarine as it approached and passed three special radio sonobuoys. The buoys were spaced to provide the maximum coverage of the scatter field in the half space above the bottom. Reception was made at each of the three buoys and at the source transducer. Sets of data were taken with the axis of the 8° source beam depressed at angles between 15° and 90°. The data were analyzed on the basis of an isotropic scatter model. Results of the spatial field were plotted in polar form, in terms of the mean scattering strength. When integration over the scattered field is performed, the ratio of power scattered from the bottom to incident power is unusual in that it is low at both low and high incident angles. The experiment resulted in the most comprehensive set of measurements of the bottom scattered field yet obtained.

PROBLEM STATUS

This is a final report on this phase of the problem; work is continuing under NRL Problem S01-47. NRL Problem S01-12 has been closed.

AUTHORIZATION

NRL Problems S01-12 and S01-47
Projects RF 101-03-44-4059, SF 101-03-15-8181, SF 11-552-006-14317,
and SF 11-552-001-8181

Manuscript submitted July 12, 1971.

THREE-DIMENSIONAL SCATTERED FIELDS FROM THE OCEAN BOTTOM

INTRODUCTION

Acoustic paths in the ocean which intersect the surface or bottom are of importance to the underwater sound community. These paths can be a source of interference in normal operations as well as be primary paths in some signaling and detection modes. Obviously the process of scattering from these boundaries should be known in order to optimize the use or rejection of these paths.

Several models have been developed, generally differing in the approximations and assumptions made, which predict the scattered field. To evaluate these models it is necessary to have experimentally determined data from a variety of bottom roughnesses and compositions. Data in the specular and monostatic directions, being the easiest to obtain, are available in abundance. Since most models predict essentially the same value in the specular direction, this allows only the monostatic point to be used to discriminate between models. Data in other directions have been obtained by only a few investigators (for example, Refs. 1-4) over limited regions of the scattered field for a limited number of surface conditions. This report presents the most comprehensive set of measurements of the bottom-scattered field yet obtained.

THEORY

The analysis of data for this report is based on the isotropic scattering model of Eckart (5) except that, following Urick (6), scattering strength is used rather than the scattering coefficient. The model states that

$$I_s = SI_iA, \tag{1}$$

where I_s is the intensity of the scattered signal referred to a unit distance (1 yard) from the boundary, S is the scattering strength, I_i is the incident intensity, and A is the insonified area contributing to the scattered signal at a particular instant.

A practical acoustic experiment employing a directive source and receiver requires an integral formulation of the received intensity I_r for fixed β (Fig. 1), namely,

$$I_r(\psi, \xi) = \int_R\int s(\delta, \psi', \xi') \left[I_0 b(\delta, \theta) \frac{10^{-Kr}}{r^{\gamma}} \right] \left[b_1(\psi', \xi') \frac{10^{-Kr'}}{r'^{\gamma'}} \right] dR, \tag{2}$$

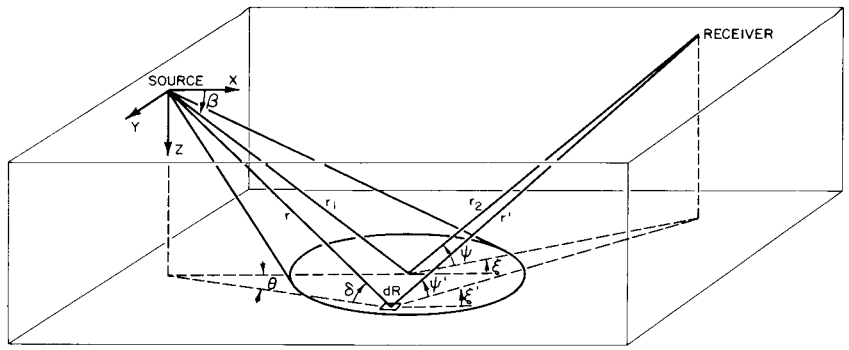

Fig. 1—Scattering geometry

where $s(\delta, \psi', \xi')$ is the scattering strength of dR* in the direction (ψ', ξ'), the first term in brackets is the incident intensity on dR, b and b_1 are the radiation functions of the source and receiver respectively, K (dB/yd) is the average absorption coefficient over the path, γ and γ'** are the effective spreading-law coefficients over the paths, and I_0 is the intensity† on the axis at unit distance from the source.

Now dR contains the factor r^2, so when we make the approximations $\gamma \approx 2$, $r \approx r_1$, and $r' \approx r_2$, Eq. (2) reduces to

$$I_r(\psi, \xi) = \frac{I_0 10^{-K(r_1+r_2)}}{r_2^{\gamma'}} \iint_R s(\delta, \psi', \xi') b(\delta, \theta) b_1(\psi', \xi') \cot \delta \, d\delta d\theta. \tag{3}$$

For the special case of monostatic reception (the receiving transducer the same as the source) Eq. (3) reduces to

$$I_r(\beta) = \frac{I_0 10^{-2kr_1}}{r_1^{\gamma'}} \iint_R s(\delta) b^2(\delta, \theta) \cot \delta \, d\delta d\theta. \tag{4}$$

For the case where the source is directional and the receiver is essentially nondirectional, $|s(\delta, \psi', \xi') - s(\beta, \psi, \xi)|$, $|\psi' - \psi|$, and $|\xi' - \xi|$ are all small for the ranges of δ and θ considered, so that, as an approximation, $s(\beta, \psi, \xi)$ may be removed from the integral and $b_1(\psi', \xi')$ = constant for the solid angle subtended by the insonified area. Then Eqs. (3) and (4) become

*It is implicitly assumed that the scattering surface is homogeneous.

**Note that the model has allowed for different spreading laws for the different paths. This is due to the dependence of spreading on the initial angle of a ray in the refractive medium. For this experiment the deviations of γ and γ' from 2 were less than ±0.01.

†I_0 can be determined from the source transmitting response L and the source current i via $I_0 = L + 20 \log i - D$ dB, where D is a loss due to the sonar dome (1 dB in our experiment).

$$I_r(\psi, \xi) = \frac{I_0 10^{-K(r_1+r_2)}}{r_2^{\gamma'}} s(\beta, \psi, \xi) b_1(\psi, \xi) \iint b(\delta, \theta) \cot \delta \, d\delta d\theta \tag{5}$$

and

$$I_r(\beta) = \frac{I_0 10^{-2Kr_1}}{r_1^{\gamma'}} s(\beta) \iint b^2(\delta, \theta) \cot \delta \, d\delta d\theta. \tag{6}$$

For $b(\delta, \theta)$ given in Fig. 2 the integrals in Eqs. (5) and (6) are -16.7 and -19.1 *dB* as calculated by the method of Appendix A in Ref. 7 (assuming steady-state conditions). Thus the scattering strength can be determined from Eqs. (5) or (6) when r_1, r_2, and γ' are determined by ray tracing and K is calculated by the method of Appendix A of this report.

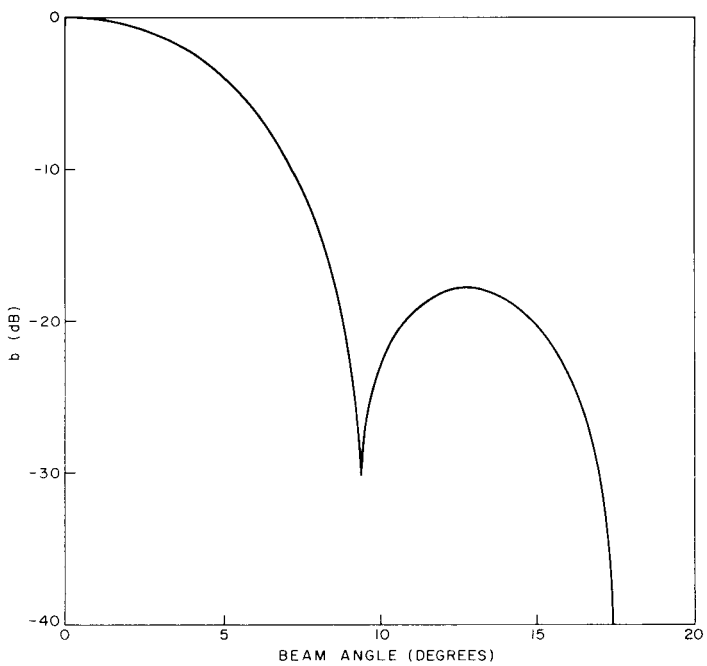

Fig. 2—Source radiation function

EXPERIMENTAL MEASUREMENTS

Area of Operations

To obtain the three-dimensional field scattered from the ocean bottom an experiment was conducted at the Blake Plateau, in the rectangular area indicated in Fig. 3. This area was chosen because of the relative flatness of the bottom, the water depth varying less than ±1 fathom over the experimental area, and because of the uniformity of the bottom material, which consisted of a calcareous sediment, as indicated by corings. Photographs of the bottom show small sand ripples with random directions.

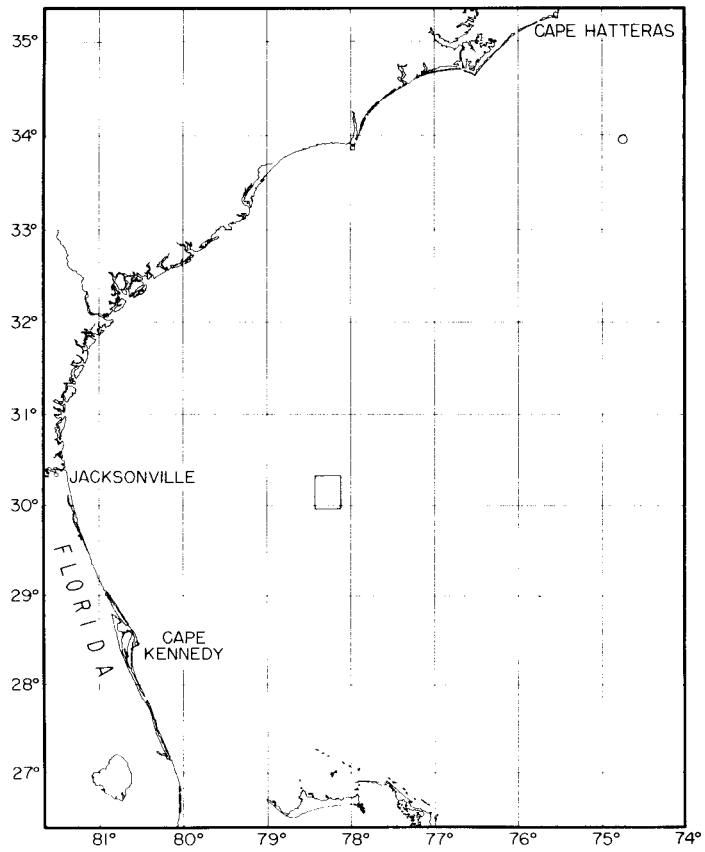

Fig. 3—Experimental area

Instrumentation

The instrumentation consisted of a special sonar operating at 19.5 kHz. The sonar included a piston transducer projecting from the bow of a submarine that could be directed throughout the forward hemisphere. Its beamwidth is approximately 8° to the half-power points, with all side lobes being down 17 dB or more. Figure 2 illustrates the directivity function between the axis and the second side lobe. The time duration of the transmitted pulses was controlled by a counter in 1-msec increments, enabling the pulse length to be varied from 2 msec to 3000 msec.

Procedure and Geometry

The return from each scattered pulse was received at four locations: the transmitting transducer and three buoy-suspended hydrophones. Relays of the signals received at the buoy hydrophones were made by HF-FM links to a ship. A typical configuration of source, receiving buoys, and ship is illustrated in Fig. 4. The runs were started with the submarine at a range of 4000 to 5000 yards from the receiving buoys. As the source progressed along the track, the scatter angles from the center of the insonified area to the receiving buoys increased until the center of the area passed the buoys and then decreased as the range was opened. The run was terminated when the

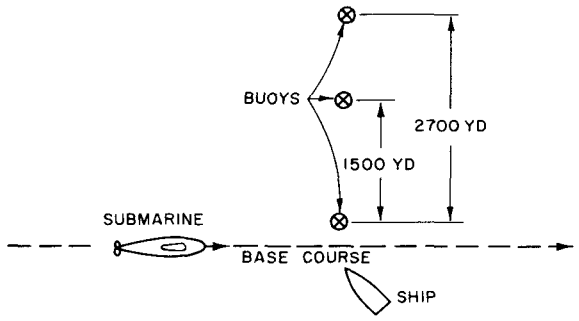

Fig. 4—Geometry of the source and the receivers

level of the signals passed into the background noise. In general this provided coverage of the hemisphere with the exception of those elevation angles lying between 0° and 15°. This limitation resulted from the refractive structure of the medium. Each of the runs were made with the depression angle of the source beam held constant throughout the run. The depression angles chosen were 15°, 30°, 45°, 60°, 70°, and 90°. Several runs were made for each depression angle.

Since the receiving buoys were free floating, it was necessary to continuously measure their individual positions relative to the source and the insonified area. This was done with an auxiliary acoustic triangulation system consisting of the source, buoys, and ship as described in Appendix B.

The entire instrumentation system was synchronized by a crystal clock in each of the two vessels. Both scattering and geometric data were recorded every 10 seconds during the runs. Details of the instrumentation system and the characteristics of the runs employed are contained in an NRL Memorandum Report (8).

Environmental data were taken periodically during the experiment to enable to computation of refractive effects of the medium in this area. These computations included the sound-speed profile, the mean sound speed over the path from the source to the center of the scatter area and the path from the center of the scatter area to the receiver as a function of the angle, the angle of arrival at the bottom as a function of the depression angle at the surface, the angle of arrival at the receiving points, the spreading loss over the paths as a function of angle, and other pertinant characteristics of the propagation.

ANALYSIS AND RESULTS

Treatment of Measured Data

The received data were analyzed to obtain the scattering strength in its appropriate direction. Values proportional to the received intensity I_r were determined from the received data, and these values were used in Eqs. (5) and (6) to obtain the scattering strengths $s(\beta,\psi,\xi)$. Since the signals received in the monostatic direction had the same scatter direction throughout each run, it was convenient to treat them as a group. The method of analysis of the data received by the source transducer is contained in Ref. 7.

For the data received at the buoys, the pressure amplitude envelope was recorded in analog form (on a dB scale) as a function of time for each of the received scatter pulses. This amplitude-envelope recording was then incremented in 10 to 25 msec steps throughout the steady-state portion of the pulse return, excluding the transient buildup and decay at the leading and trailing edges, and converted from analog to digital form with the aid of a data reader. Each pulse was thus broken down into n increments, and each incremental digital value (designated e_i, $i = 1, \ldots, n$) was then squared to give a power ratio. The power ratios were averaged over the number of increments in each return:

$$<e^2> = \frac{1}{n} \sum_{i=1}^{n} e_i^2 . \tag{7}$$

The mean value of the envelope was then converted to dB by

$$<E> = 10 \log <e^2>. \tag{8}$$

This makes $<E> \propto <I>$, assuming that intensity is proportional to pressure squared.

Scattered Field

The mean scattering strength $s(\beta, \psi, \xi)$ for each scattered pulse was then computed using Eqs. (5) and (8). From the symmetry of the experiment to either side of the specular plane, the data in $180° \leqslant \xi \leqslant 360°$ (Fig. 1) were folded back into the region $0 \leqslant \xi \leqslant 180°$. Most of the data were averaged over increments of 10° in azimuth and elevation to provide sufficient quantities for statistical treatment. The only exceptions were the monostatic data points and the data for 90° incidence. The data at 90° are independent of azimuth, as confirmed by inspection. This independence enabled the data to be averaged over 2° increments in elevation.

Thus s is an average of several mean returns. Along with s the logarithmic standard deviation (LSD) of the mean returns was calculated:

$$LSD = 10 \log \left(1 + \frac{\sigma}{\mu}\right),$$

where $\sigma = \sigma(<E>)$ and $\mu = \mu(<E>)$.

Figure 5 presents plots of s versus elevation angle of those data falling between 0° and 10° in azimuth for incident angles of about 15°, 30°, 45°, 60°, 70° and 90°. (The incident angles differed somewhat from the depression angles due to refraction.) In all these plots the maximum level of scatter appears in or near the specular direction as expected. Figure 6 is a plot of the LSD corresponding to the data for the 90°-incident case shown in Fig. 5f. There appears to be a decrease in variation as the scatter angle is increased.

The scattering strengths for other angles of azimuth are presented in the first section of Appendix C.

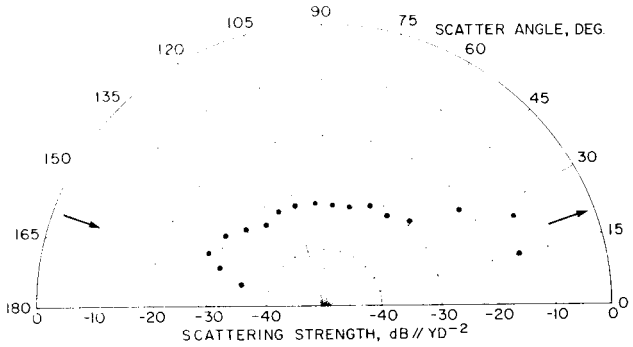

(a) Angle of incidence 19.7°

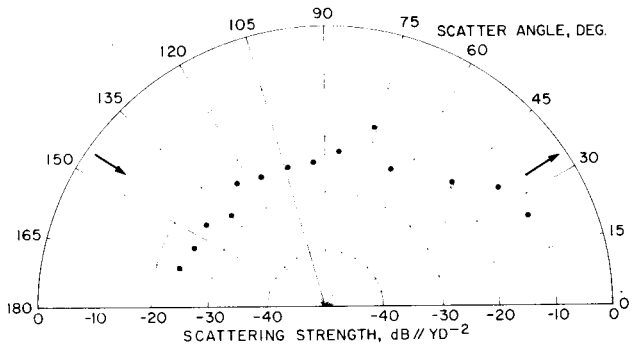

(b) Angle of incidence 32.4°

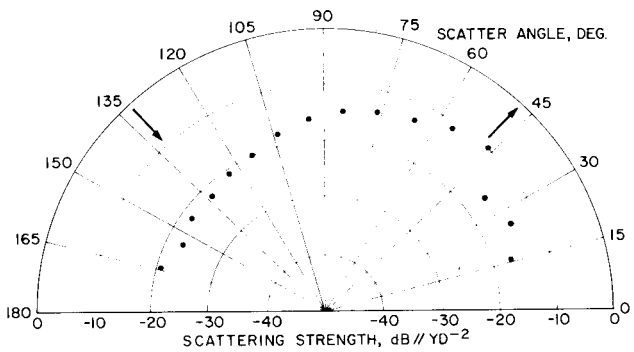

(c) Angle of incidence 46.4°

Fig. 5—Scattering strength in the specular plane (±10° in azimuth).

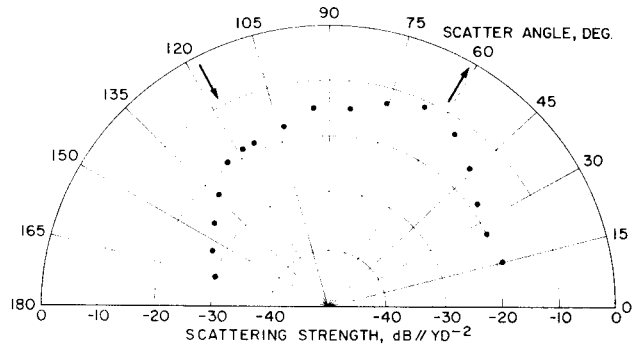

(d) Angle of incidence 60.8°

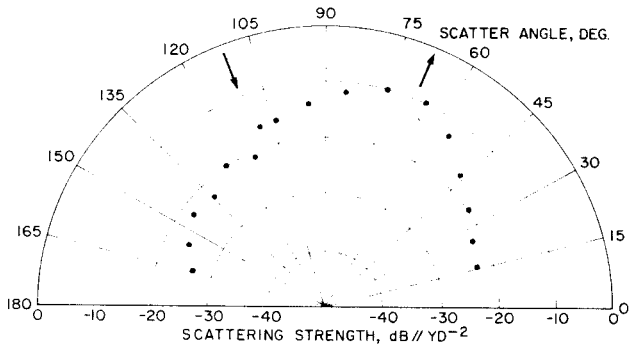

(e) Angle of incidence 70.5°

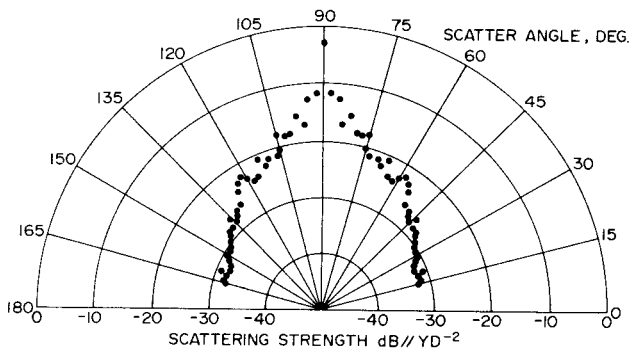

(f) Angle of incidence 90.0°

Fig. 5—Scattering strength in the specular plane (±10° in azimuth)—(Continued).

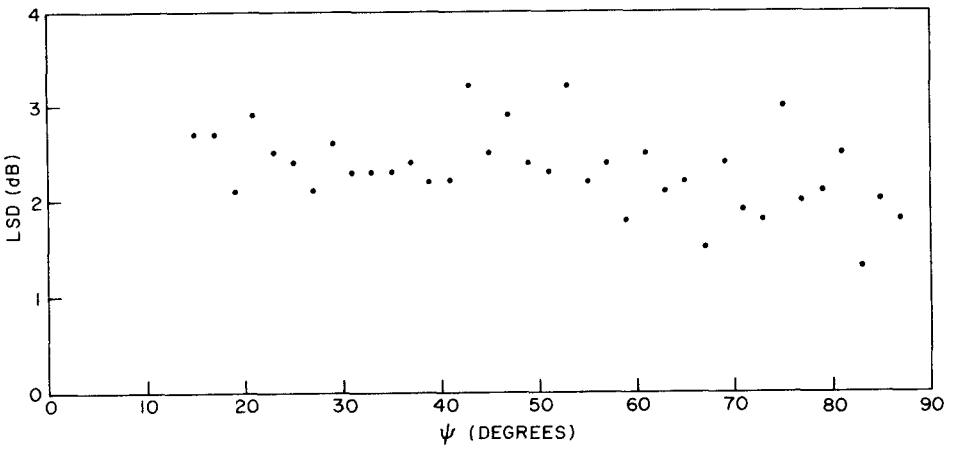

Fig. 6—Logarithmic standard deviation of the average values in Fig. 5f

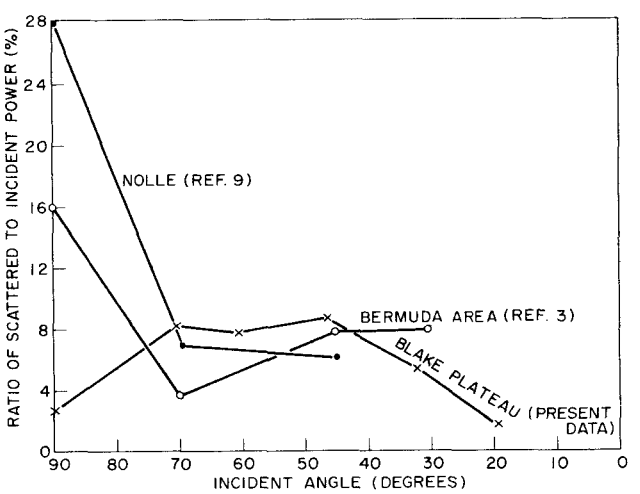

Fig. 7—Computed ratio of scattered to incident power as a function of the incident angle.

Ratio of Scattered to Incident Power

A numerical integration of $s(\beta, \psi, \xi)$ over a unit hemisphere gives that fraction of the incident power that is scattered from the bottom back into the water. The values in Appendix C were smoothed, interpolated, and extrapolated to obtain a complete coverage of the upper half space. Then the data were numerically integrated as shown in the second section of Appendix C. The results are presented in Fig. 7 as the curve labeled Blake Plateau. The curve labeled Bermuda is the result of previous work of this group. The curve labeled Nolle is our integration of data as reported by Nole *et al.* (9) for laboratory experiments on graded sands at 1 MHz. Since the Nolle data were given only for an azimuth angle of 0°, it was necessary to assume symmetry about the specular direction.

An example of the three-dimensional shape of the scattered field is illustrated by the paper model in Fig. 13, which is for 70° incidence and is not logarithmically compressed, as are the other results presented. This model was constructed from data that had been smoothed and interpolated. The line entering the base from the right indicates the incident angle and from the left at the peak, indicates the specular direction.

SUMMARY AND CONCLUSIONS

An experiment was performed which gives wide coverage of the three-dimensional scatter field. The scattered field for an incident angle of 90° (Fig. 5f), being independent of azimuth angle, is a fairly complete description of the field. The scattered field is much more directive than the image field from a smooth surface would be, as the source was about 8° wide at the 3-dB-down points and the field is approximately 4° wide at the 10-dB down points. This increased directivity is not present in the scattered fields at other angles of incidence. It is felt that the directivity is there but was not measured because the field was not sampled at a suffiently fine mesh.

Fig. 8—Three-dimensional model of the scattered field for an angle of incidence of 70.5°. The incident and specular directions are indicated by the wires

When the scattered fields are integrated over the upper half space, the result is the normalized scattered power (Fig. 7). The amount of power scattered back is small, less than 9% maximum, and the amount of scattered power drops rapidly for both low and high incident angles. The drop for low incident angles would be less if the hypothesized (but unnoticed) directivity increase were present.

ACKNOWLEDGEMENT

The Commander, Operational Test Evaluation Force, provided the ship and submarine to aid in the acquisition of data for the experimental portion of this report. The USS *Rockville* (EPCER-851) and USS *Grouper* (AGSS-214) were available 18 days operating and in transit plus 10 days at the pier for installation and removal of instrumentation.

REFERENCES

1. R.J. Urick, "The Backscattering of Sound from a Harbor Bottom," *J. Acoust. Soc. Amer.* **26**, 231 (1954).

2. A.W. Nolle, W.A. Hoyer, J.F. Mifsud, W.R. Runyan, and M.B. Ward, "Acoustical Properties of Water Filled Sands," *J. Acoust. Soc. Amer.* **35**, 1394 (1963).

3. B.G. Hurdle, K.D. Flowers, and D.P. Thompson, "Bistatic Acoustic Scattering from the Ocean Bottom," *NRL Report* **7285** (1971).

4. C.W. Horton, S.K. Mitchell, and G.R. Barnard, "Model Studies of the Scattering of Acoustic Waves from a Rough Surface," *J. Acoust. Soc. Amer.* **41**, 635 (1967).

5. C. Eckart, "Principles and Applications of Underwater Sound," *NDRC Summary Technical Reports*, Division 6, Volume 7, Washington, D.C. (1946).

6. R.J. Urick, "The Backscattering of Sound from a Harbor Bottom," *J. Acoust. Soc. Amer.* **26**, 231 (1954).

7. B.G. Hurdle and K.D. Flowers, "Effect of Geometry on Acoustic Monostatic Scattering from the Ocean Bottom," *NRL Report* **6517** (1967).

8. H.U. Criss, K.D. Flowers, B.G. Hurdle, R.M. Lee, and K.P. Thompson, "Procedures for a Series of Experiments in Acoustic Scattering from the Ocean Bottom and Volume in the Blake Plateau Area," *NRL Memorandum Report* **1767** (1967).

9. A.W. Nolle, W.A. Hoyer, J.F. Mifsud, W.R. Runyan, and M.B. Ward, "Acoustical Properties of Water Filled Sands," *J. Acoust. Soc. Amer.* **35**, 1394 (1963).

APPENDIX A

EFFECTS OF PROPAGATION

REFRACTIVE EFFECTS

The positioning system discussed in Appendix B fixed all of the receiving sensors with respect to the submarine. Since a sound-velocity structure is present in the medium, positioning with respect to the scattering area becomes more complicated. However, given an initial direction of propagation, ray tracing through the medium locates the position of the insonified area with respect to the submarine. It then remains to determine that unique ray which connects the center of the insonified area and each of the receiving sensors. Also computed are the angles (azimuth and elevation) that the ray makes when leaving the insonified area and when received at the sensor and the spreading losses over these paths. All of the computations were made using Horton's* equations in a ray-trace program in which the sound-speed profile was divided into a number of linear segments.

ABSORPTION

To obtain the average attenuation coefficient K over the path, a numerical integration over the depth divided by the depth was made. Thus $K = 10 \log \langle K \rangle$, where

$$\langle K \rangle = \frac{1}{d} \int_0^d k(z)\, dz,$$

in which $k(z)$ is the function relating absorption and depth. In determining $k(z)$ the temperature, salinity, and pressure were taken into account. The value of K used in the analysis was 2.268×10^{-3} dB/yd.**

*J.W. Horton, "Fundamentals of Sonar," U.S. Naval Institute, Navships 92719 (1957).

**B.G. Hurdle, K.D. Flowers, and K.P. Thompson, "Bistatic Acoustic Scattering from the Ocean Bottom," NRL Report 7285 (1971);

APPENDIX B

MONITORING POSITIONS BY ACOUSTIC MEANS

In making the scattering strength measurements at sea with a number of acoustic sensors to obtain the three-dimensional field, it was necessary to know the relative positions of the sensors and source fairly accurately. Then, since the insonified area on the bottom was always fixed with respect to the submarine, the positions of the receiving sensors with respect to the insonified area were known. Knowing the actual spatial positions of the insonified area and the sensors, ray paths between them were calculated and the associated angles determined. To obtain the relative positions of the sensors and source an auxiliary acoustic system was developed to measure the geometry illustrated in Fig. B1. Ranges R_1 through R_7 and the angle α were recorded simultaneously with each acoustical scattering measurement.

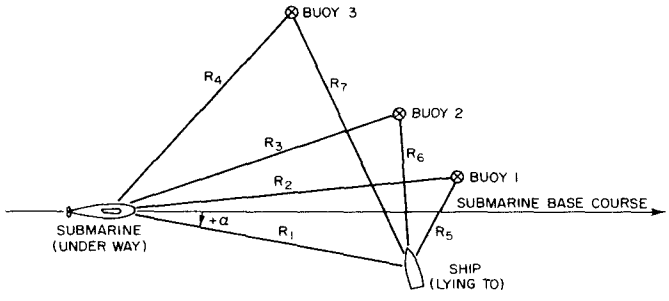

Fig. B1—Sonar ranges (obtained automatically every 10 seconds) and periscope bearing α to the ship (manually recorded every minute).

The angle α was measured with the periscope of the submarine. To accomplish the range measurements, a 25-kHz source on the submarine transmitted a 1-msec pulse every 10 seconds; at the same time a 14-kHz source on the ship transmitted a similar pulse. The buoys received and then retransmitted these signals by HF-FM links to the ship. From knowledge of speed of sound in the surface region and the elapsed time over the different paths, ranges R_1 through R_2 were obtained.

The counters, which started to count elapsed time in milliseconds at the same time the pulses originated, were stopped when a received signal level surpassed a preset threshold. The number in the counter was then read out and the counter zeroed just prior to the beginning of the next 10-second interval. The count (in milliseconds) was then recorded on punched paper tape. An example of one run of this type of data is given in Fig. B2. Range in time or yards is the ordinate and the abscissa is time of transmission. As expected the ranges R_1 through R_4 are approximate hyperbolas (their deviations are caused by submarine course variations and drift of the receiving sensors) and the ranges R_5 through R_7 are approximate straight lines. The range curves R_5 through R_7 are essentially parallel and in this case, increase in range with time due to the ship drifting faster than the buoys.

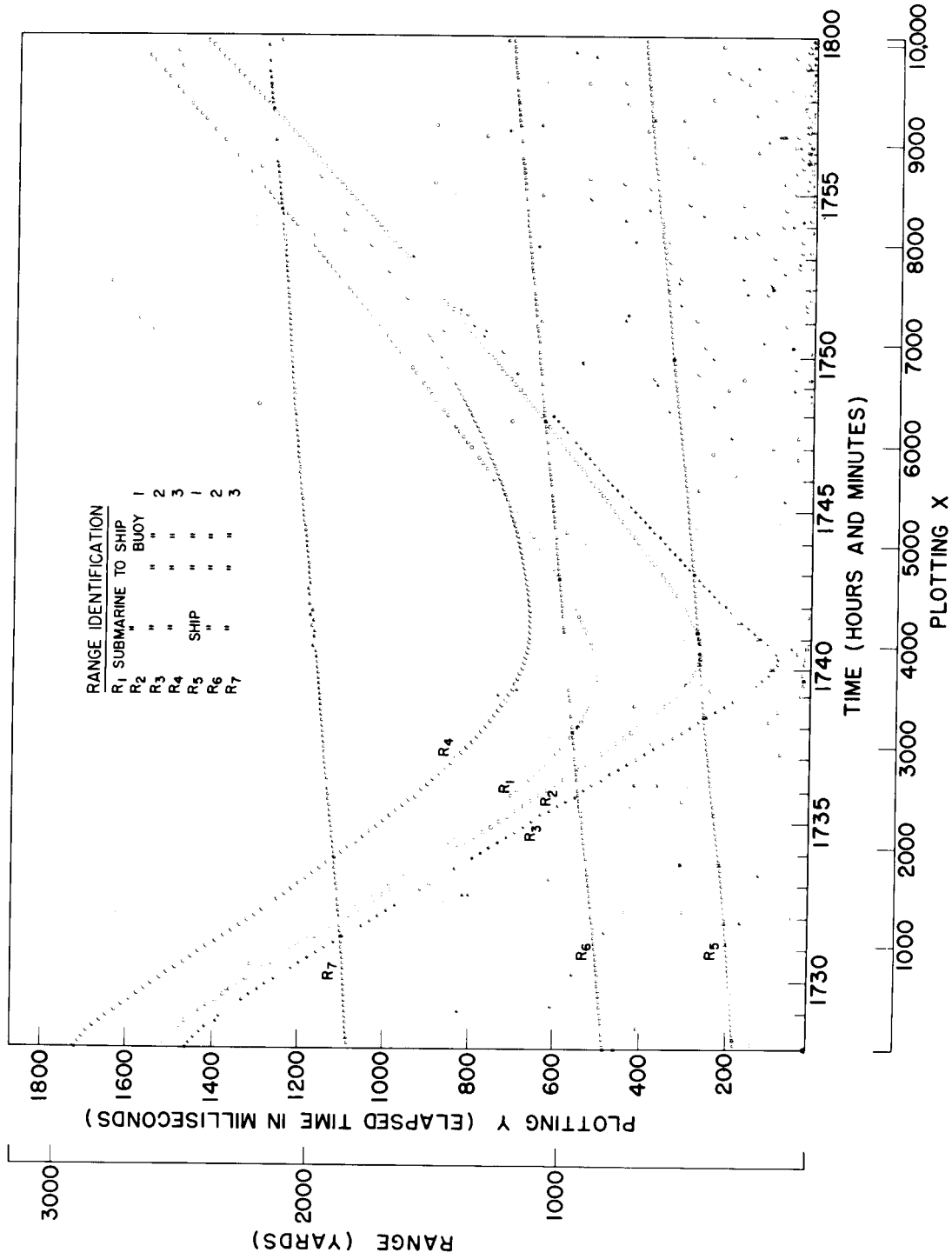

Fig. B2—Horizontal ranges (identified in Fig. B1) versus time for Run 11; original data

As can be seen the counters were sometimes stopped by noise bursts, but it was unusual for the counter not to be stopped by the pulse if it was not stopped by noise before the pulse arrives. Missing points were subsequently filled in by linear interpolation for R_5 through R_7 and by hyperbolic interpolation or extrapolation on ranges R_1 through R_4.

Thus for each set of the range measurements, with the depth and location of the scattering area known, the azimuth and elevation of each receiving point with respect to the center of the scattering area were obtained, using the technique of Appendix A of NRL Report 6517.*

*B.G. Hurdle and K.D. Flowers, "Effect of Geometry on Acoustic Monostatic Scattering from the Ocean Bottom," NRL Report 6517 (1967).

APPENDIX C

THREE-DIMENSIONAL DATA

AVERAGE VALUES OF $s(\beta, \psi, \xi)$

The data presented in Figs. C1 through C5 consist of values of $s(\beta, \psi, \xi)$ for β values of about 15°, 30°, 45°, 60°, and 75°. Each figure can be considered a top view of half of a hemispherical dome. The elevation angle ψ is divided into nine 10° steps and the azimuth angle ξ is divided into eighteen 10° steps. The values of $s(\beta, \psi, \xi)$ for $180° \leqslant \xi \leqslant 360°$ are assumed to be the same as the reflected values of $s(\beta, \psi, \xi)$ for $0 \leqslant \xi \leqslant 180°$, with the axis of symmetry being the (0, 180°) azimuth line.

In each figure the incident angle (or monostatic scatter direction) is marked by an X and the center of the insonified area is beneath the pole and at the point of convergence of the radial azimuth lines. A number in a 10° stop area is the average value of $s(\beta, \psi, \xi)$ in that direction. Figures 5 of the main text are plots of the points found between 0° and 90° elevation, 0° and 10° azimuth, and 170° and 180° azimuth. In some cases the data in Figs. C1 through C5 were extrapolated from nearby data, as is most noticeable in the case of β = 60° (Fig. C4) between 170° and 180° azimuth.

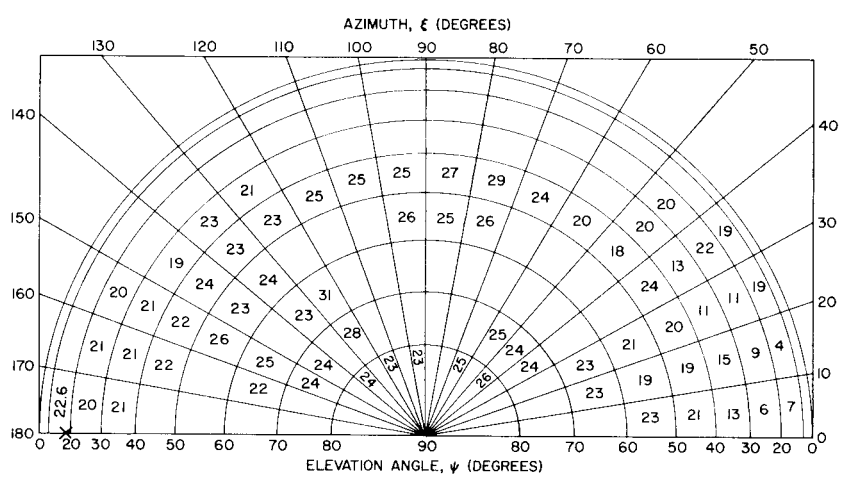

Fig. C1—Scattering strength in the upper half space for an angle of incidence of 19.7°. The field is assumed symmetrical on either side of the specular plane. (The specular plane is perpendicular to the page along the lower edge of the plot; Fig. 5a is a side view of this plane.) The incident angle is marked with an X, and the center of the scattering area is directly beneath the pole. The blank 10°-step areas are due to missing values.

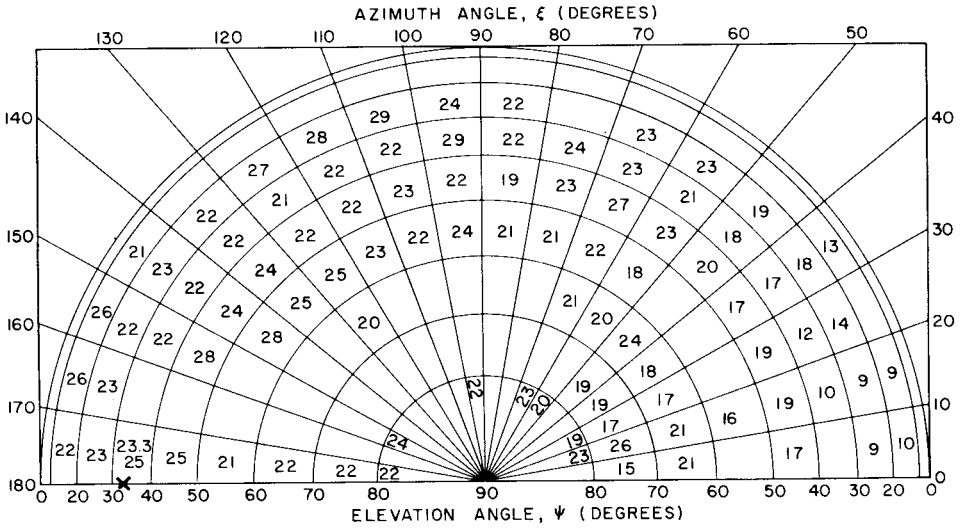

Fig. C2—Scattering strength in the upper half space for an angle of incidence of 32.4°.

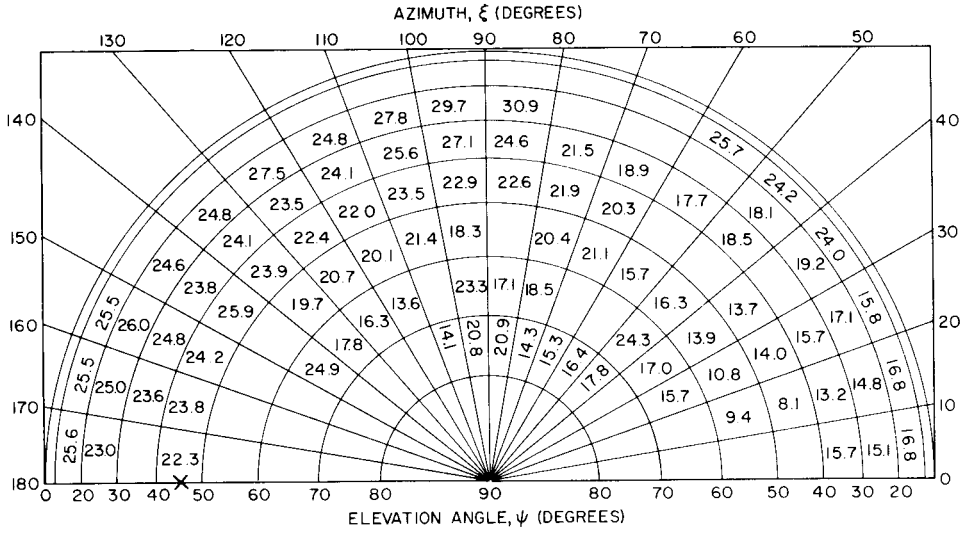

Fig. C3—Scattering strength in the upper half space for an angle of incidence of 46.4°.

COMPUTATION OF SCATTERED POWER

The data were interpolated and extrapolated to fill in all the missing areas. The resulting values of $s(\beta, \psi, \xi)$ were then integrated over a unit hemisphere, giving the ratio of the scattered power to the incident power as a function only of β. That is

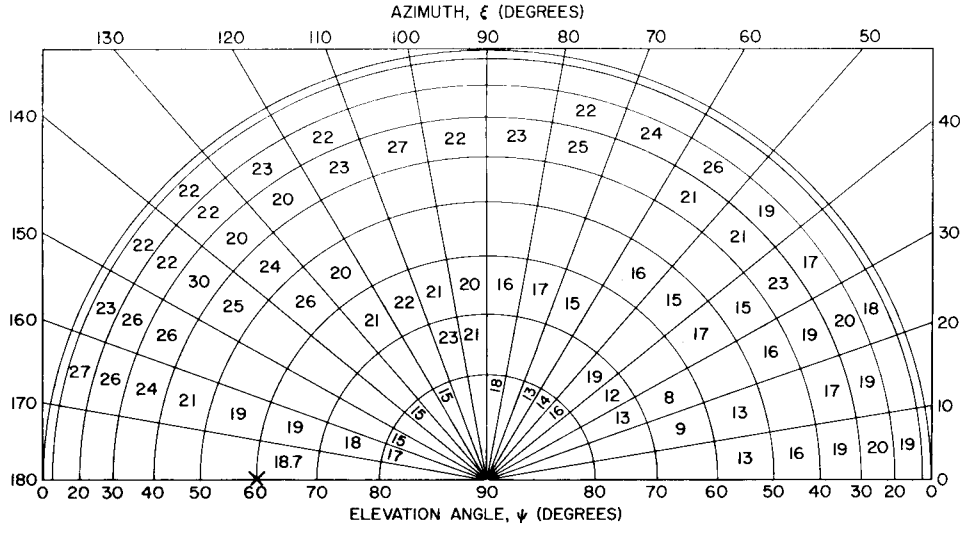

Fig. C4—Scattering strength in the upper half space for an angle of incidence of 60.8°.

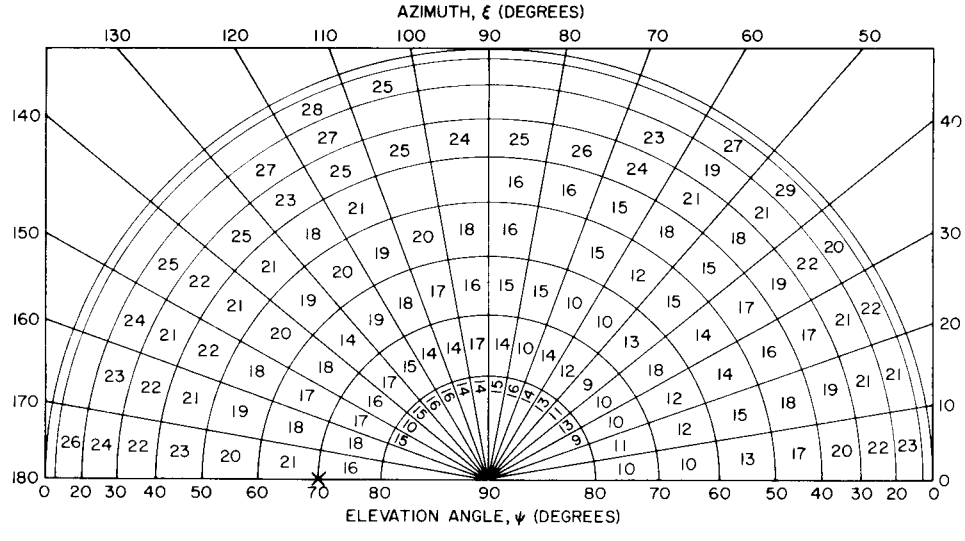

Fig. C5—Scattering strength in the upper half space for an angle of incidence of 70.5°.

$$\frac{P(\beta)_{\text{scattered}}}{P_{\text{incident}}} = \int_0^{2\pi} \int_0^{\pi/2} s(\beta, \psi, \xi) \cos \psi \, d\psi d\xi$$

$$= 2 \int_0^{\pi} \int_0^{\pi/2} s(\beta, \psi, \xi) \cos \psi \, d\psi d\xi.$$

This integral was numerically evaluated from

$$\frac{P(\beta)_{\text{scattered}}}{P_{\text{incident}}} = 2 \sum_{j=1}^{18} \sum_{i=1}^{9} s(\beta, \overline{\psi}_i, \overline{\xi}_j)(\sin \psi_i - \sin \psi_{i-1})(\xi_j - \xi_{j-1})$$

$$= \frac{\pi}{9} \sum_{j=1}^{18} \sum_{i=1}^{9} s(\beta, \overline{\psi}_i, \overline{\xi}_j)(\sin \psi_i - \sin \psi_{i-1})$$

where

$$\psi_i = i\Delta\psi = i(10^\circ), \qquad i = 1, ..., 9,$$

$$\xi_j = j\Delta\xi = j(10^\circ), \qquad j = 1, ..., 18,$$

$$\overline{\psi}_i = (\psi_i + \psi_{i-1})/2,$$

$$\overline{\xi}_j = (\xi_j + \xi_{j-1})/2.$$

The results of this evaluation are presented in Fig. 7.

Security Classification

DOCUMENT CONTROL DATA - R & D

(Security classification of title, body of abstract and indexing annotation must be entered when the overall report is classified)

1. ORIGINATING ACTIVITY *(Corporate author)* Naval Research Laboratory Washington, D.C. 20390	2a. REPORT SECURITY CLASSIFICATION Unclassified 2b. GROUP

3. REPORT TITLE

THREE-DIMENSIONAL SCATTERED FIELDS FROM THE OCEAN BOTTOM

4. DESCRIPTIVE NOTES *(Type of report and inclusive dates)* A final report on one phase of the NRL Problems. Problem S01-12 is closed; work continues under NRL Problem S01-47.

5. AUTHOR(S) *(First name, middle initial, last name)*

Kenneth D. Flowers, Burton G. Hurdle, and Kingsley P. Thompson

6. REPORT DATE November 5, 1971	7a. TOTAL NO. OF PAGES 24	7b. NO. OF REFS 9
8a. CONTRACT OR GRANT NO. NRL Problems S01-12 and S01-47 b. PROJECT NO. RF 101-03-44-4059, SF 101-03-15-8181 c. SF 11-552-006-14317, SF 11-552-001-8181 d.	9a. ORIGINATOR'S REPORT NUMBER(S) NRL Report 7325 9b. OTHER REPORT NO(S) *(Any other numbers that may be assigned this report)*	

10. DISTRIBUTION STATEMENT

Approved for public release; distribution unlimited

11. SUPPLEMENTARY NOTES	12. SPONSORING MILITARY ACTIVITY Department of the Navy, Office of Naval Research, Arlington, Va. 22217 and Naval Ship Systems Command, Washington, D.C. 20360

13. ABSTRACT

An experiment to determine the three-dimensional acoustic field scattered from the sea bottom was conducted in the Blake Plateau. Pulsed 19.5-kHz transmissions were directed toward the bottom from a submarine as it approached and passed three special radio sonobuoys. The buoys were spaced to provide the maximum coverage of the scatter field in the half space above the bottom. Reception was made at each of the three buoys and at the source transducer. Sets of data were taken with the axis of the 8° source beam depressed at angles between 15° and 90°. The data were analyzed on the basis of an isotropic scatter model. Results of the spatial field were plotted in polar form, in terms of the mean scattering strength. When integration over the scattered field is performed, the ratio of power scattered from the bottom to incident power is unusual in that it is low at both low and high incident angles. The experiment resulted in the most comprehensive set of measurements of the bottom-scattered field yet obtained.

DD FORM 1 NOV 65 1473 (PAGE 1)

S/N 0101-807-6801

Security Classification

14. KEY WORDS	LINK A ROLE	LINK A WT	LINK B ROLE	LINK B WT	LINK C ROLE	LINK C WT
Underwater acoustics						
Ocean bottom						
Acoustic scattering						
Sonar						